Manuscript prepared for The Cryosphere
with version 5.0 of the LaTeX class copernicus.cls.
Date: 10 July 2015

Evaluation of the updated regional climate model RACMO2.3: summer snowfall impact on the Greenland Ice Sheet

B. Noël[1], W.J. van de Berg[1], E. van Meijgaard[2], P. Kuipers Munneke[1], R. S. W. van de Wal[1], and M.R. van den Broeke[1]

[1]Institute for Marine and Atmospheric research Utrecht, University of Utrecht, Netherlands
[2]Royal Netherlands Meteorological Institute, De Bilt, Netherlands

Correspondence to: Brice Noël (B.P.Y.Noel@uu.nl)

Abstract.

We discuss Greenland ice sheet (GrIS) surface mass balance (SMB) differences between the updated polar version of the regional climate model RACMO2.3 and the previous version RACMO2.1. Among other revisions, the updated model includes an adjusted rainfall-to-snowfall conversion, producing exclusively snowfall under freezing conditions; this especially favours snowfall in summer. Summer snowfall in the ablation zone of the GrIS has a pronounced effect on melt rates, affecting modelled GrIS SMB in two ways. By covering relatively dark ice with highly reflective fresh snow, these summer snowfalls have the potential to locally reduce melt rates in the ablation zone of the GrIS through the snow-albedo-melt feedback. At larger scales, SMB changes are driven by differences in orographic precipitation following a shift in large-scale circulation, in combination with enhanced moisture to precipitation conversion for warm to moderately cold conditions. A detailed comparison of model output with observations from automatic weather stations, ice cores and ablation stakes shows that the model update generally improves the simulated SMB-elevation gradient as well as the representation of the surface energy balance, although significant biases remain.

1 Introduction

Since the mid-1990s, atmospheric and oceanic warming in the Arctic has led to accelerated Greenland ice sheet (GrIS) mass loss (Enderlin and Howat, 2013; Fettweis et al., 2013; Wouters et al., 2013). Combined observational and model studies show that increased meltwater runoff, and solid ice discharge through the acceleration of marine-terminating outlet glaciers (Hanna et al., 2009; Nick et al., 2009; Fettweis et al., 2011; Rignot et al., 2011), account for $\sim 60\%$ and $\sim 40\%$ of the recent GrIS mass loss, respectively (Rignot et al., 2008; Van den Broeke et al., 2009; Enderlin and Howat, 2013).

Since surface melt over the GrIS is mainly driven by the absorption of shortwave radiation (Van den Broeke et al., 2008), surface albedo is a primary factor governing ice sheet surface mass balance (SMB) (Bougamont et al., 2005; Tedesco et al., 2011; Fitzgerald et al., 2012) and surface energy balance (SEB) (Tedesco et al., 2008; Van Angelen et al., 2012). Ice albedo is mainly a function of impurity content, while snow albedo is sensitive to several snow physical properties, e.g. grain size, liquid water content and soot concentration. Satellite and in-situ observations have revealed a general decay of GrIS surface albedo in recent years (Box et al., 2012; Stroeve et al., 2013). In the ablation zone, this decrease is mainly caused by the prolonged exposure of dark, bare ice (Fettweis et al., 2011; Tedesco et al., 2011). In the accumulation zone, it is proposed that higher temperatures lead to enhanced snow metamorphism and surface darkening (Box et al., 2012), resulting in enhanced melt through the positive melt-albedo feedback (Stroeve, 2001).

Summer snowfall events can interrupt this feedback, by covering dark ice and/or metamorphosed snow with a highly reflective fresh snow layer. Greuell and Oerlemans (1986) showed that significant summer snowfall events ($>$ 5 mmWE) on an Alpine glacier caused a major reduction in ablation during the following days, subsequently leading to a long-term positive SMB anomaly. They estimated this positive SMB response to be two to three times larger than the mass of deposited solid precipitation. Fettweis et al. (2005) analysed two heavy snowfall events in southeast Greenland at the end of July 1991, using MAR (Modèle Atmosphérique Régional) and AVHRR satellite imagery. These events temporarily raised surface albedo, delaying the appearance of darker bare ice. Based on data from automatic weather stations (AWS), Van den Broeke et al. (2011) showed that even

minor summer snowfall events (< 5 mmWE) can considerably reduce surface melting.

Therefore, an accurate representation of (summer) snowfall events is essential to model the SMB of the GrIS (Fettweis et al., 2005; Van Angelen et al., 2012). This requires a high-resolution model, to resolve the narrow ablation zone, and an explicit model of atmospheric and surface snow/ice physics. Here, we use the polar version of the regional atmospheric climate model RACMO2.3, at 11 km horizontal resolution, which is coupled to a multilayer snow model with prognostic albedo formulation. We compare the simulated GrIS SMB and SEB with the previous model version (RACMO2.1, Van Angelen et al. (2012)) and with ice cores, stake and AWS measurements along the K-transect in west Greenland, with special reference to the representation of summer snowfalls. In Section 2, the physics upgrades in RACMO2.3 and the measurements along the K-transect are briefly described. The impact of upgraded physics on GrIS SMB through the snow-albedo feedback is discussed in Section 3. Section 4 evaluates model output using K-transect and accumulation zone data, after which conclusions are drawn in Section 5.

2 Model and data

2.1 The regional climate model RACMO2

The Regional Atmospheric Climate Model (RACMO2) is developed and maintained at the Royal Netherlands Meteorological Institute (KNMI) (Van Meijgaard et al., 2008). RACMO2 adopts the atmospheric physics module from the European Centre for Medium-range Weather Forecasts Integrated Forecast System (ECMWF-IFS) and the dynamical core of the High Resolution Limited Area Model (HIRLAM) (Undèn et al., 2002). The polar version of RACMO2 was developed by the Institute for Marine and Atmospheric Research (IMAU), Utrecht University to specifically represent the SMB evolution over the ice sheets of Greenland, Antarctica and other glaciated regions. To that end, the atmosphere model has been interactively coupled to a multilayer snow model that simulates meltwater percolation, refreezing and runoff (Ettema et al., 2010). It includes an albedo scheme with prognostic snow grain size (Kuipers Munneke et al., 2011) and a drifting snow routine that simulates interactions between drifting snow, the ice sheet surface and the lower atmosphere (Lenaerts et al., 2012).

2.2 RACMO2.3 update

The RACMO2 physics package has recently been updated from cycle CY23r4 used in RACMO2.1 (White, 2001) to cycle CY33r1 in the current RACMO2.3 version (ECMWF-IFS, 2008). These updates include major changes in the description of cloud microphysics, surface and boundary layer turbulence, and radiation transport (Van Wessem et al., 2014). The updated physics package includes an eddy-diffusivity mass flux scheme (Siebesma et al., 2007), representing turbulence and shallow convection in the atmospheric boundary layer. The surface flux computation is based on Monin-Obukhov similarity theory (Beljaars et al., 2004). The new radiation scheme McRad (Morcrette et al., 2008), based on the Monte Carlo independent column approximation (Barker et al., 2008), computes the shortwave and longwave radiation transmission through clouds. In addition, the interaction of shortwave or longwave radiation with multilayered clouds has been improved by revising the cloud optical properties (ECMWF-IFS, 2008).

The new cloud scheme includes an ice supersaturation parameterisation, which prolongs the vapour phase at low temperatures (Tompkins et al., 2007). The auto-conversion coefficient, controlling the conversion rate of water-vapour into precipitation in convective clouds, has been defined individually for liquid and ice water clouds, following Sundqvist (1978). Moreover, under marginally freezing conditions, i.e. between -7°C and -1°C, precipitation occurs exclusively as snowfall even though the precipitating clouds are mixed phase. In the previous model version, similar atmospheric conditions could also have resulted in a mix of liquid and solid precipitation for temperatures above -7°C. The update results in improved relative contributions of rainfall and snowfall to the total precipitation flux (Lin et al., 1983). Furthermore, the cloud water-to-snowfall conversion coefficient now remains constant for liquid (> 0°C) and mixed phase clouds (-23°C to 0°C) whereas it decreases with temperature for ice clouds (< -23°C), resulting in slower snowfall production. The cloud content to ice and liquid water conversion coefficients have been increased in CY33r1 to reduce the overestimated updraft condensation simulated in previous cycles, leading to enhanced convective precipitations (ECMWF-IFS, 2008; Van Wessem et al., 2014). Other minor adjustments have been applied to the physics package and the dynamical core but these are not relevant for this study. A complete overview of all updates is provided by ECMWF-IFS (2008) and Van Meijgaard et al. (2012).

2.3 RACMO2 simulations set-up

In the polar version of RACMO2.3, identical domain and resolutions (∼ 11 km, 40 vertical layers) were used as in the previous RACMO2.1 simulation (Van Angelen et al., 2013). The integration domain includes the GrIS, the Canadian Arctic Archipelago, Iceland and Svalbard. At the lateral atmospheric boundaries, RACMO2.3 is forced at 6-hourly time interval by reanalysis data of ERA-40 (Uppala et al., 2005) for the period 1958-1978 and ERA-Interim (Stark et al., 2007; Dee et al., 2011) for the period 1979-2014. Sea surface temperature and sea ice cover are prescribed from the same reanalysis data. Since RAMCO2.1 has been forced by ERA-Interim data only for the period 1990-2012 and by ERA-40 prior to that, we compare model results for the overlap-

ping period (1990-2012). This period coincides with long-term SMB and AWS measurements performed along the K-transect in west Greenland, which are therefore also used for model evaluation (see Section 2.4) together with accumulation data from ice cores covering the same period.

In both RACMO2 versions, Moderate Resolution Imaging Spectroradiometer (MODIS) albedo products (Stroeve et al., 2005) are used to prescribe a background ice albedo, which is assumed to vary in space but to be constant in time. MODIS products were retrieved from satellite observations at 0.05 degree spatial and 8 day temporal resolutions. The background ice albedo field (Fig. 1) is based on 2001-2010 MODIS values, and ranges from 0.30 to 0.55.

2.4 Observational data

For model evaluation, we use long-term measurements from the K-transect, operated by the Institute for Marine and Atmospheric Research of Utrecht University in the Netherlands. The K-transect runs for a distance of approximately 140 km from the ice margin through the ablation zone and into the lower accumulation zone of the west Greenland ice sheet along $\sim 67°$N, covering the elevation interval between 400 m a.s.l. and 1850 m a.s.l. (Fig. 1, white dots). Since 1990, annual stake measurements have been performed at eight sites along the transect: S4, S5, SHR, S6, S7, S8, S9 and S10 (Van de Wal et al., 2005, 2012). Since August 2003, three AWS with capability to close the SEB have been operated at sites S5 ($\sim$ 500 m a.s.l.), S6 ($\sim$ 1000 m a.s.l.) and S9 ($\sim$ 1500 m a.s.l.) (Van den Broeke et al., 2008, 2009, 2011). Stations S5 and S6 are located in the ablation zone at about 5 km and 40 km from the ice sheet margin, while station S9 is located close to the equilibrium line at approximately 90 km from the ice sheet margin. Since 2011, an AWS is also operated in the accumulation zone at S10 ($\sim$ 1850 m), about 140 km from the ice sheet margin. At this location, data consist of a merged time series collected at KAN_U in 2010 and S10 for 2011-2012. At the AWS sites, SEB components are computed using a SEB model that uses as input hourly mean observations of wind, temperature, humidity and radiation components (Van den Broeke et al., 2011). The model evaluation also includes a comparison with accumulation measurements collected at 87 sites (Fig. 1, yellow dots). This dataset is based on a compilation of deep snow pits and firn cores measurements presented in Bales et al. (2001, 2009), selected only when temporal overlap.

To compare model to observations, we apply a distinct selection method in the ablation and accumulation zones of the GrIS. In the accumulation zone, modelled SMB is obtained by selecting the closest RACMO2 grid cell. Due to significant dependence of ablation terms on elevation, modelled SMB and SEB components were retrieved by successively selecting the nearest grid cell and then applying an altitude correction. To do so, we select a grid cell, among the closest pixel and its 8 adjacent neighbours, which minimizes the elevation bias between the model and the stations.

3 Changes in SMB components

3.1 SMB change pattern

Fig. 2 shows a) RACMO2.3 average SMB (1990-2012) and b) the difference in SMB between RACMO2.3 and RACMO2.1. Both model versions simulate a qualitatively realistic SMB field, with a narrow ablation zone fringing the ice sheet (Fig. 2). The ablation zone is widest ($\sim$ 100-150 km) in the southwest and northeast, but too narrow in the southeast to be resolved at a resolution of 11 km; in this part of the ice sheet, the steep topography and high precipitation rates induce a large SMB gradient, resulting in an ablation zone only a few km wide.

The SMB fields from RACMO2.1 and RACMO2.3 are qualitatively similar, but two patterns of change can be discerned (Fig. 2b). First, a large-scale pattern with decreased SMB in the west and increased SMB in the east results in enhanced longitudinal SMB gradients across the main topographical divide. The negative SMB change becomes gradually more pronounced towards the southern and southeastern ice sheet, while the positive anomalies peak in the east. This large-scale pattern can be attributed to changes in the general circulation over the GrIS, as developed in Section 3.2.

Secondly, superimposed on this large-scale pattern, Fig. 2b shows pronounced positive SMB changes that are spatially restricted to the ablation and lower accumulation zones of the south-western and north-eastern ice sheet. These regional changes can be ascribed to enhanced summer snowfall in RACMO2.3, following the revised rainfall to snowfall partitioning. These changes are discussed in detail in Section 3.3.

3.2 Large-scale precipitation changes

The average mid-tropospheric circulation at 500 hPa is directed from southwest to northeast over Greenland (Fig. 3a), resulting in a large-scale precipitation gradient in the same direction. In addition, the vicinity of the polar front, which predominantly produces easterly flow to its north, causes depressions to propagate eastward towards southern Greenland. This leads to a pronounced topographically forced precipitation maximum along the southeastern coast.

Relative to RACMO2.1, RACMO2.3 is 0.1 to 0.3°C colder in the upper troposphere (above 500 hPa, not shown). Among other processes, reduced upper-air condensation, attributed to the introduction of ice supersaturation in the updated physics, contributes to this cooling. Moreover, a lowering of the 500 hPa geopotential height is modelled over the ice sheet with a minimum situated over coastal southeast Greenland (Fig. 3b). The resulting cyclonic circulation anomaly results in stronger onshore flow and increased precipitation in

the north-eastern GrIS and a decrease in the northwestern ice sheet, on the lee side of the main divide. In south Greenland, RACMO2.3 simulates decreased precipitation with respect to the previous model version; this is related to enhanced north-westerly advection of colder and drier air masses on the western side of the divide, more frequent offshore katabatic circulation and consequently weakened onshore flow to the east (Noël et al., 2014).

The large-scale circulation anomaly also reduces evaporation over the north Atlantic Ocean, by up to 200 mmWE per year (not shown). Moreover, because condensation in the updated scheme is enhanced for moderately cold conditions ($< 10°C$), precipitation over the ocean is enhanced, further limiting precipitation in coastal southeast Greenland. Precipitation differences locally reach 25%, and integrated over the GrIS the average 1990-2012 precipitation is reduced by 6%, from 741 Gt/yr in RACMO2.1 to 698 Gt/yr in RACMO2.3. Note that the erratic box-like pattern in Fig. 3b results from an error in the meridional momentum advection scheme in RACMO2.1, which is solved in the current formulation.

3.3 Summer snowfall events: the snow-albedo-melt feedback

Owing to an increase of the cloud water-to-snowfall conversion coefficient, the revised physics in RACMO2.3 favours solid precipitation at the expense of liquid precipitation, especially for cloud temperatures between -7°C and -1°C. In winter this has no major impact on the rainfall/snowfall ratio because the air temperature remains mostly below the solid precipitation threshold. In summer (JJA), however, RACMO2.3 predicts locally enhanced snowfall (10-40 mmWE), notably in southwest, northeast and northwest Greenland (Fig. 4a). These regional changes are accompanied by an equivalent decrease in rainfall (Fig. 4b), so we conclude that they result from the updated precipitation scheme. The reduced summer snowfall in the centre and southeast and the increase in east Greenland are not compensated by opposite and equivalent rainfall changes; here, precipitation changes are caused by the circulation change discussed in Subsection 3.2.

The regions experiencing increased summer snowfall coincide with positive changes in JJA surface albedo (Fig. 4c). The impact of summer snowfall on albedo is largest in the ablation zone, where the amount of absorbed shortwave radiation is reduced by a factor of ~ 3 when dark bare ice (albedo $\sim$ 0.30 - 0.55) is covered by fresh snow (albedo $\sim$ 0.85). As a consequence, meltwater runoff, which in RACMO2 is assumed to occur instantaneously over bare ice, is also substantially reduced (Fig. 4d). Note that this reduction in runoff (40-160 mmWE) significantly exceeds in magnitude the snowfall anomaly in Fig. 4a (5-30 mmWE), stressing the importance of the snow-albedo-melt feedback mechanism, in line with previously published results for valley glaciers (Greuell and Oerlemans, 1986). The pronounced runoff reductions are mirrored in the map of SMB change (Fig. 2b).

4 Evaluation using observational data

4.1 SEB evaluation along the K-transect

In this section, we compare modelled and observed monthly mean SEB components (2004-2012) along the K-transect, conveniently situated in a region of west Greenland where there are significant differences in SMB between the two model versions (Fig. 2b). We adopted the convention of positive energy fluxes when directed towards the surface. The melt flux (M, W m^{-2}) is given by:

$$\begin{aligned} M &= SWd + SWu + LWd + LWu + SHF + LHF + Gs \\ &= SWn + LWn + SHF + LHF + Gs \end{aligned}$$

where: SWd and SWu are the downward and upward shortwave radiation fluxes (W m^{-2}), LWd and LWu are the downward and upward longwave radiation fluxes (W m^{-2}), SHF and LHF are the sensible and latent turbulent heat fluxes (W m^{-2}), and SWn and LWn are the net short/longwave radiation fluxes (W m^{-2}), and Gs is the subsurface heat flux (W m^{-2}) which remains small, i.e. not exceeding -1.43 W m^{-2} yr^{-1}, and is not further discussed in this paper.

SEB data from the AWS at S6 are not used because of gaps in the time series. Fig. 5 and Tables 1 to 3 show observed and modelled monthly mean SEB components, surface albedo, melt energy and the differences for the period 2004-2012 (S5 and S9) and 2010-2012 (S10). For station S9, a distinction is made between the sub-periods 2004-2008 and 2009-2012; this is deemed relevant because of the significantly warmer summer conditions near the surface and in the upper atmosphere during the latter period. Figs. 5a, c, e and g show that there is qualitative agreement between the modelled and observed seasonal cycle of the SEB in the ablation, equilibrium and accumulation zones. However, important biases remain, as discussed below.

4.1.1 Ablation zone (S5)

At station S5, Table 1 shows that both RACMO2 versions significantly overestimate SWd and underestimate LWd, even more so in RACMO2.3, which is indicative of underestimated cloud optical thickness. In combination with underestimated ice albedo (Fig. 5b) this leads to significantly overestimated net shortwave radiation (SWn) in summer (Fig. 5a). On the other hand, RACMO2 underestimates the large summertime SHF values at S5, although this is improved in RACMO2.3 (Table 1). The reason is that station S5 has a complex topography: neither the summertime advection of warm tundra air over the glacier tongue that protrudes onto the tundra, leading to underestimated air temperature (Table 1), nor the high surface roughness at the marginal

glaciers (Smeets and van den Broeke, 2008) is well described at 11 km resolution. This leads to underestimated surface to air gradients of temperature and wind, and hence too small SHF. This does not strongly affect LHF, which remains close to zero at S5. The net effect on melt energy is a negative bias (Fig. 5b) that has become smaller in RACMO2.3 (from 18 to 13%), albeit owing to significant error compensation.

4.1.2 Around the equilibrium line (S9)

At S9, RACMO2.3 reduces the bias in most SEB components (Table 2). The 2 meter temperature bias has almost vanished, which has improved the representation of SHF. Despite a notable improvement of winter LWn (not shown), LWd remains underestimated (Table 2). Average biases in SWd, SWu and SWn are greatly reduced in RACMO2.3. In RACMO2.1, the average melt bias was small at S9 (Table 2), but this was the result of overestimated melt in the period 2004-2008, and underestimated melt in 2009-2012 (Fig. 5d and f). For the period 2004-2008, enhanced summer snowfall has increased surface albedo in RACMO2.3 (Fig. 6a), which leads to an overall improved representation and a clearly reduced melt bias (Fig. 5d). In contrast, simulated summer snowfall has not considerably changed at station S9 for the period 2009-2012 (Fig. 6b) and biases in albedo and melt energy have persisted (Fig. 5d and f). The explanation is that summer atmospheric temperatures in 2009-2012 were too high for the new precipitation scheme to enhance snowfall.

The bias in surface albedo between model and observations (Fig. 5f) can be explained by the too high prescribed bare ice albedo (Fig. 1). No ice albedo could be derived from MODIS imagery for this location, in which case we prescribe a constant ice albedo of 0.55. However, in recent warm summers, the surface at S9 showed lower albedo values of $\sim$ 0.43 and $\sim$ 0.45 in 2010 and 2012, respectively. As a consequence, both RACMO2 versions fail to capture this ongoing decline of summer ice albedo.

4.1.3 Accumulation zone (S10)

At S10, biases in shortwave fluxes are greatly reduced but again the negative LWd bias persists (Table 3). In winter this is mainly compensated by an overestimated SHF, but not so in summer (Fig. 5g). In June and July, the representation of albedo has improved, but in August albedo is now overestimated. SWn remains somewhat too large. However, since LWn is underestimated, the errors in melt energy are less than 10 W m^{-2} (Fig. 5h). The lower accumulation zone responds similarly to station S9 during 2004-2008 but with a reduced surface albedo sensitivity to summer snowfall, because snow metamorphism is slower in this colder area and snow wetting occurs less frequently.

The generally improved representation of surface snow albedo is attributed to enhanced summer snowfall in RACMO2.3 (see Section 3.3), thickening the melting snow cover and allowing the snow layer to persist longer over bare ice areas in summer. As a result, snowmelt decreases, further delaying snow cover disappearance and maintaining the surface albedo high until summer snowfall events cease (Fig. 6a). The summer surface albedo increase is further reinforced by a drop in cloud cover. This process reduces LWd, also decreasing snowmelt at station S9 (Fig. 5d).

4.2 SMB evaluation

4.2.1 Temporal SMB variability

Table 4 compares time series of modelled and measured annual SMB values (1990-2012) collected at 7 stake sites, ranging from station S5 in the lower ablation zone to station S10 in the accumulation zone (Fig. 1, white dots). Fig. 7 shows these time series for RACMO2.3 at four sites. The lowermost stake S4 ($\sim$ 400 m a.s.l.) is excluded from the analysis because it is not well resolved by the model ice sheet mask. At all sites except S10, the agreement improves in RACMO2.3, expressed as lower biases and a higher percentage of variance explained (r^2, Table 4). At S10, SMB inter-annual variability is not well captured, but it must be stated that stake SMB measurements have limited accuracy in the percolation zone due to uncertainties in the snow density and subsurface refreezing.

4.2.2 Spatial SMB variability

Fig. 8 compares modelled and observed SMB in the GrIS accumulation zone retrieved from snow pits and firn cores (Fig. 1, yellow dots). In the accumulation zone, the difference in modelled SMB between both RACMO2 versions (Fig. 2b) is mostly driven by changes in precipitation (Fig. 3b). Relative to the previous model version, RACMO2.3 simulates wetter conditions in central and northeast Greenland whereas the southern region shows reduced precipitation. These changes improve the agreement with accumulation measurements at most locations in the accumulation zone (Fig. 8).

Table 4 and Fig. 9 compare modelled and observed K-transect average SMB (1991-2012) as deduced from annual stake measurements. Fig. 9 also shows the prescribed MODIS background albedo (green dots, scale on right axis). The covariance of ice albedo with modelled SMB once more underlines the importance of ice albedo for the ablation zone SMB (Van Angelen et al., 2012). Again it must be noted that the stake sites are not necessarily representative for a larger region, e.g. for the area of a model grid cell ($\sim$ 120 km^2).

In the lower ablation zone, between 500 to 800 m a.s.l., RACMO2.3 simulates lower (more negative) SMB values than RACMO2.1, which better matches observations. This improvement can be ascribed to a smaller bias in melt energy (Table 1) and hence a more realistic runoff. Correcting the persistent overestimation of SMB between 500 m a.s.l.

and 800 m a.s.l. will require a better representation of SHF which, in combination with SWd and LWd, is a primary factor governing melt rate in the lower ablation zone. For elevations between 800 m and the equilibrium line at about 1500 m a.s.l., RACMO2.3 simulates higher SMB values compared to RACMO2.1, resulting mainly from reduced runoff following enhanced summer snowfall through the snow-albedo-melt feedback. The absence of rapid SMB fluctuations in the model between 1400 m a.s.l. and the equilibrium line is clearly related to the fixed upper threshold (0.55) of bare ice albedo prescribed in RACMO2 (Van Angelen et al., 2012). In the accumulation zone (above 1500 m), enhanced snowfall and less runoff have significantly improved the agreement with the K-transect stake observations.

An alternative way to assess model performance is to quantify SMB gradients, here determined by simple least-squares fitting of a linear function. This yields 3.15 $\pm$ 0.22 mmWE yr^{-1} m^{-1} for the observations and 2.73 $\pm$ 0.09 and 2.91 $\pm$ 0.07 mmWE yr^{-1} m^{-1} for RACMO2.1 and RACMO2.3, respectively; in the updated model, the deviation from the observed gradient has thus decreased from 0.42 to 0.24 mmWE yr^{-1} m^{-1}, a 43% improvement of the SMB gradient representation.

5 Conclusions

An updated physics package has been implemented in the regional climate model RACMO2.3. Among other changes, the rainfall-to-snowfall conversion has been revised and an ice supersaturation parameterization included, to favour solid over liquid precipitation in summer and reduce the overestimated coastal cloud cover and precipitation simulated in previous versions, respectively (Van de Berg et al., 2006). The subsequent increase in modelled summer snowfall has generally improved the representation of surface energy balance (SEB) and surface mass balance (SMB) along the K-transect in west Greenland. For SEB, these improvements are more pronounced in the lower accumulation zone, where summer temperatures are generally below zero. Close to the equilibrium line, SMB is especially sensitive to snowfall-induced fluctuations in surface albedo. The increase in summer snowfall enhances surface reflectivity, improving the modelled surface albedo in summer as well as SMB representation. However, in recent warm years (e.g. 2010 and 2012) rainfall prevailed even in the new formulation, and no improvement was obtained. At station S5 in the lower ablation zone, summer albedo in RACMO2 is mainly determined by the prescribed MODIS ice albedo, due to near-continuous bare ice exposure. The updated physics in RACMO2.3 have considerably improved the modelled SMB gradient along the K-transect when compared to ablation stake measurements, reducing the bias by 43%.

Two remaining problems require particular attention in future model updates. Current RCMs still struggle to model the correct cloud cover and cloud type (ice/water) over the GrIS (Box et al., 2012). For instance, both RACMO2 and MAR models underestimate summer LWd and overestimate SWd due to an underestimated cloud optical thickness (Ettema et al., 2010; Fettweis et al., 2011). In fact, the inclusion of ice supersaturation in RACMO2.3 might aggravate this problem over the ablation zone, because, for inland-propagating air masses, this process delays cloud condensation to higher ice sheet elevations, as was also seen in simulations of Antarctic climate (Van Wessem et al., 2014). Evaluation of the modelled cloud properties and surface properties using CloudSAT/Calypso data will be addressed in a forthcoming paper.

Another revision that is simpler to implement is improvement of the background ice albedo, that is currently too low at the ice sheet margin. However, at this point, it is also important to realize that point AWS (SEB) and stake (SMB) measurements may not be representative for a wider area, especially for a spatially heterogeneous variable such as surface albedo. Sub-grid albedo variability should therefore become an important future topic of study. To assess the quality of the simulated SMB in the ablation zone elsewhere in Greenland, an evaluation of downscaled RACMO2.3 data against a much larger dataset of ablation measurements, covering all sectors of the Greenland ice sheet, is currently being conducted.

Acknowledgements. B. Noël, W. J. van de Berg, P. Kuipers Munneke, R. S. W. van de Wal, and M. R. van den Broeke acknowledge support from the Polar Programme of the Netherlands Organization for Scientific Research (NWO/ALW)

References

R. C. Bales, J. R. McConnell, E. Mosley-Thompson, and B. Csatho. Accumulation over the greenland ice sheet from historcal and recent records. *Journal of Geophysical Research*, 106(D24):33813 – 33825, 2001. doi:10.1029/2001JD900153.

R. C. Bales, Q. Guo, D. Shen, J. R. McConnell, G. Du, J. F. Burkhart, V. B. Spikes, E. Hanna, and J. Cappelen. Annual accumulation for greenland updated using ice core data developed during 2000–2006 and analysis of daily coastal meteorological data. *Journal of Geophysical Research*, 114(D6):D06116, 2009. doi:10.1029/2008JD011208.

H. W. Barker, J. N. S. Cole, J-J. Morcrette, R. Pincus, P. Räisänen, K. von Salzenf, and P. A. Vaillancourtg. The Monte Carlo Independent Column Approximation: An assessment using several global atmospheric models. *Quarterly Journal of the Royal Meteorological Society*, 134:1463 – 1478, 2008. doi:10.1002/qj.303.

A. C. M. Beljaars, A. R. Brown, and N. Wood. A new parametrization of turbulent orographic form drag. *Quarterly Journal of the Royal Meteorological Society*, 130:1327 – 1347, 2004. doi:10.1256/qj.03.73.

M. Bougamont, J. L. Bamber, and W. Greuell. A surface mass balance model for the Greenland Ice Sheet. *Journal of Geophysical Research*, 110:F04018, 2005. doi:10.1029/2005JF000348.

J. E. Box, X. Fettweis, d M. Tedesco J. C. Stroeve a, D. K. Hall, and K. Steffen. Greenland ice sheet albedo feedback: thermodynamics and atmospheric drivers. *The Cryosphere*, 6:821 – 839, 2012. doi:10.5194/tc-6-821-2012.

D. P. Dee, S. M. Uppala, A. J. Simmons, P. Berrisford, P. Poli, S. Kobayashi, U. Andrae, M. A. Balmaseda, G. Balsamo, P. Bauer, P. Bechtold, A. C. M. Beljaars, L. van de Berg, J. Bidlot, N. Bormann, C. Delsol, R. Dragani, M. Fuentes, A. J. Geer, L. Haimberger, S. B. Healy, H. Hersbach, E. V. Hólm, L. Isaksen, P. Kållberg, M. Köhler, M. Matricardi, A. P. McNally, B. M. Monge-Sanz, J.-J. Morcrette, B.-K. Park, C. Peubey, P. de Rosnay, C. Tavolato, J.-N. Thépaut, and F. Vitart. The ERA-Interim reanalysis: configuration and performance of the data assimilation system. *Quarterly Journal of the Royal Meteorological Society*, 137:553 – 597, 2011. doi:10.1002/qj.828.

ECMWF-IFS. Part IV : PHYSICAL PROCESSES (CY33R1). *Technical Report*, 2008.

E. M. Enderlin and I. M. Howat. Submarine melt rate estimates for floating termini of greenland outlet glaciers (2000–2010). *Journal of Glaciology*, 59:67 – 75, 2013. doi:10.3189/2013JoG12J049.

J. Ettema, M. R. van den Broeke, E. van Meijgaard, W. J. van de Berg, J. E. Box, and K. Steffen. Climate of the Greenland ice sheet using a high-resolution climate model – Part 1: Evaluation. *The Cryosphere*, 4:511 – 527, 2010. doi:10.5194/tc-4-511-2010.

X. Fettweis, H. Gallée, F. Lefebre, and J.-P. van Ypersele. Greenland surface mass balance simulated by a regional climate model and comparison with satellite-derived data in 1990-1991. *Climate Dynamics*, 24:623 – 640, 2005. doi:10.1007/s00382-005-0010-y.

X. Fettweis, M. Tedesco, M. van den Broeke, and J. Ettema. Melting trends over the Greenland ice sheet (1958-2009) from spaceborne microwave data and regional climate models. *The Cryosphere*, 5: 359 – 375, 2011. doi:10.5194/tc-5-359-2011.

X. Fettweis, E. Hanna, C. Lang, A. Belleflamme, M. Erpicum, and H. Gallée. Brief communication: Important role of the mid-tropospheric atmospheric circulation in the recent surface melt increase over the Greenland ice sheet. *The Cryosphere*, 7:241 – 248, 2013. doi:10.5194/tc-7-241-2013.

P. W. Fitzgerald, J. L. Bamber, J. K. Ridley, and J. C. Rougier. Exploration of parametric uncertainty in a Surface Mass Balance Model applied to the Greenland Ice Sheet. *Journal of Geophysical Research*, 117:F01021, 2012. doi:10.1029/2011JF002067.

W. Greuell and J. Oerlemans. Sensitivity studies with a mass balance model including temperature profile calculations inside the glacier. *Zeitschrift für Gletscherkunde und Glazialgeologie*, 22: 101 – 124, 1986. ISSN 0044-2836.

E. Hanna, J. Cappelen, X. Fettweis, P. Huybrechts, A. Luckman, and M. H. Ribergaard. Hydrologic response of the Greenland ice sheet: the role of oceanographic warming. *Hydrological Processes*, 23:7 – 30, 2009. doi:10.1002/hyp.7090.

P. Kuipers Munneke, M. R. van den Broeke, J. T. M. Lenaerts, M. G. Flanner, A. S. Gardner, and W. J. van de Berg. A new albedo parameterization for use in climate models over the Antarctic ice sheet. *Journal of Geophysical Research*, 116:D05114, 2011. doi:10.1029/2010JD015113.

J. T. M. Lenaerts, M. R. van den Broeke, J. H. Angelen, E. van Meijgaard, and S. J. Déry. Drifting snow climate of the Greenland ice sheet: a study with a regional climate model. *The Cryosphere Discussion*, 6:1611 – 1635, 2012. doi:10.5194/tcd-6-1611-2012.

Y-L. Lin, R. D. Farley, and H. D. Orville. Bulk Parameterization of the Snow Field in a Cloud Model. *Journal of Applied Meteorology*, 22:1065 – 1092, 1983. doi:10.1175/1520-0450(1983)022<1065:BPOTSF>2.0.CO;2.

J-J. Morcrette, H. W. Barker, J. N. S. Cole, M. J. Iacono, and R. Pincus. Impact of a new radiation package, McRad, in the ECMWF integrated forecast system. *Monthly Weather Review*, 136:4773 – 4798, 2008. doi:10.1175/2008MWR2363.1.

F. M. Nick, A. Vieli, I. M. Howat, and I. Joughin. Large-scale changes in Greenland outlet glacier dynamics triggered at the terminus. *Nature Geoscience*, 2:110 – 114, 2009. doi:10.1038/ngeo394.

B. Noël, X. Fettweis, W. J. van de Berg, M. R. van den Broeke, and M. Erpicum. Sensitivity of Greenland Ice Sheet surface mass balance to perturbations in sea surface temperature and sea ice cover: a study with the regional climate model MAR. *The Cryosphere*, 8:1871 – 1883, 2014. doi:10.5194/tc-8-1871-2014.

E. Rignot, J. E. Box, E. Burgess, and E. Hanna. Mass balance of the Greenland ice sheet from 1958 to 2007. *The Cryosphere*, 35: L20502, 2008. doi:10.1029/2008GL035417.

E. Rignot, I. Velicogna, M. R. van den Broeke, A. Monaghan, and J. Lenaerts. Acceleration of the contribution of the Greenland and Antarctic ice. *Geophysical Research Letters*, 38:L05503/1 – L05503/5, 2011. doi:10.1029/2011GL046583.

A. P. Siebesma, P. M. M. Soares, and J. Teixeira. A combined Eddy-Diffusivity Mass-Flux Approach for the Convective Boundary Layer. *Journal of the Atmospheric Sciences*, 64:1230 – 1248, 2007. doi:http://dx.doi.org/10.1175/JAS3888.1.

C.J.P.P. Smeets and M.R. van den Broeke. Temporal and Spatial Variations of the Aerodynamic Roughness Length in the Ablation Zone of the Greenland Ice Sheet. *Boundary Layer Meteorology*, 128:315 – 338, 2008. doi:10.1007/s10546-008-9291-0.

J. D. Stark, Exeter Met Office, C. J. Donlon, M. J. Martin, and M. E. McCulloch. OSTIA: An operational, high resolution, real time, global sea surface temperature analysis system. *OCEANS 2007 - Europe*, pages 1 – 4, 2007. doi:10.1109/OCEANSE.2007.4302251. Conference Publications.

J. Stroeve, J. E. Box, F. Gao, S. L. Liang, A. Nolin, and C. Schaaf. Accuracy assessment of the MODIS 16-day albedo product for snow: comparisons with Greenland in situ measurements. *Remote Sensing of Environment*, 94:46 – 60, 2005. doi:10.1016/j.rse.2004.09.011.

J. Stroeve, J. E. Box, Z. Wang, C. Schaafc, and A. Barretta. Re-evaluation of MODIS MCD43 Greenland albedo accuracy and trends. *Remote Sensing of Environment*, 138:199 – 214, 2013. doi:10.1016/j.rse.2013.07.023.

J. C. Stroeve. Assessment of Greenland albedo variability from the advanced very high resolution radiometer Polar Pathfinder data set. *Journal of Geophysical Research*, 106:360 – 374, 2001. doi:10.1016/S0034-4257(00)00179-6.

H. Sundqvist. A parameterization scheme for non-convective condensation including prediction of cloud water content. *Quarterly Journal of the Royal Meteorological Society*, 104:677 – 690, 1978. doi:10.1002/qj.49710444110.

M. Tedesco, M. Serreze, and X. Fettweis. Diagnosing the extreme surface melt event over southwestern Greenland in 2007. *The Cryosphere*, 2:159 – 166, 2008. doi:10.5194/tc-2-159-2008.

M. Tedesco, X. Fettweis, M. R. van den Broeke, R. S. W. van de Wal, C. J. P. P. Smeets, W. J. van de Berg, M. C. Serreze, and J. E. Box. The role of albedo and accumulation in the 2010 melting record in Greenland. *Environmental Research Letters*, 6:014005, 2011. doi:10.1088/1748-9326/6/1/014005.

A. M. Tompkins, K. Gierens, and G. Rädel. Ice supersaturation in the ECMWF integrated forecast system. *Quarterly Journal of the Royal Meteorological Society*, 133:53 – 63, 2007. doi:10.1002/qj.14.

P. Undèn, L. Rontu, H. Järvinen, P. Lynch, J. Calvo, G. Cats, J. Cuxart, K. Eerola, C. Fortelius, J. A. Garcia-Moya, C. Jones, G. Lenderlink, A. Mcdonald, R. Mcgrath, B. Navascues, N. W. Nielsen, V. Degaard, E. Rodriguez, M. Rummukainen, K. Sattler, B. H. Sass, H. Savijarvi, B. W. Schreur, R. Sigg, and H. The. HIRLAM-5. *Scientific Documentation*, 2002. Technical Report.

S. M. Uppala, P. W. KÅllberg, A. J. Simmons, U. Andrae, V. Da Costa Bechtold, M. Fiorino, J. K. Gibson, J. Haseler, A. Hernandez, G. A. Kelly, X. Li, K. Onogi, S. Saarinen, N. Sokka, R. P. Allan, E. Andersson, K. Arpe, M. A. Balmaseda, A. C. M. Beljaars, L. Van De Berg, J. Bidlot, N. Bormann, S. Caires, F. Chevallier, A. Dethof, M. Dragosavac, M. Fisher, M. Fuentes, S. Hagemann, E. Hólm, B. J. Hoskins, L. Isaksen, P. A. E. M. Janssen, R. Jenne, A. P. Mcnally, J-F. Mahfouf, J-J. Morcrette, N. A. Rayner, R. W. Saunders, P. Simon, A. Ster, K. E. Trenberth, A. Untch, D. Vasiljevic, P. Viterbo, and J. Woollen. The ERA-40 re-analysis. *Quarterly Journal of the Royal Meteorological Society*, 131:2961 – 3012, 2005.

J. H. Van Angelen, J. T. M. Lenaerts, S. Lhermitte, X. Fettweis, P. Kuipers Munneke, M. R. van den Broeke, E. van Meijgaard, and C. J. P. P. Smeets. Sensitivity of Greenland Ice Sheet surface mass balance to surface albedo parameterization: a study with a regional climate model. *The Cryosphere*, 6:1175 – 1186, 2012. doi:10.5194/tc-6-1175-2012.

J. H. Van Angelen, M. R. van den Broeke, B. Wouters, and J. T. M. Lenaerts. Contemporary (1969-2012) evolution of the climate and surface mass balance of the Greenland ice sheet. *Surveys in Geophysics*, 2013. doi:10.1007/s10712-013-9261-z.

W.J. Van de Berg, M.R. van den Broeke, C.H. Reijmer, and E. van Meijgaard. Reassessment of the Antarctic surface mass balance using calibrated output of a regional atmospheric climate model. *Journal of Geophysical Research*, 111:D11104, 2006. doi:10.1029/2005JD006495.

R. S. W. Van de Wal, W. Boot, C. J. P. P. Smeets, H. Snellen, M. R. van den Broeke, and J. Oerlemans. Twenty-one years of mass balance observations along the K-transect, West Greenland. *Earth System Science Data*, 4:31 – 35, 2012. doi:10.5194/essdd-5-351-2012.

R.S.W. Van de Wal, W. Greuell, M. R. van den Broeke, C. H. Reijmer, and J. Oerlemans. Surface mass-balance observations and automatic weather station data along a transect near Kangerlussuaq, West Greenland. *Annals of Glaciology*, 42:311 – 316, 2005. doi:10.3189/172756405781812529.

M. R. Van den Broeke, P. Smeets, J. Ettema, and P. Kuipers Munneke. Surface radiation balance in the ablation zone of the west Greenland ice sheet. *Journal of Geophysical Research: Atmospheres*, 113:D13105, 2008. doi:10.1029/2007JD009283.

M. R. Van den Broeke, P. Smeets, and J. Ettema. Surface layer climate and turbulent exchange in the ablation zone of the west Greenland ice sheet. *International Journal of Climatology*, 29: 2309 – 2323, 2009. doi:10.1002/joc.1815.

M. R. Van den Broeke, P. Smeets, and R. S. W. van de Wal. The seasonal cycle and interannual variability of surface energy balance and melt in the ablation zone of the west Greenland ice sheet. *The Cryosphere*, 5:377 – 390, 2011. doi:10.5194/tc-5-377-2011.

E. Van Meijgaard, L. H. van Ulft, W. J. van de Berg, F. C. Bosveld, B. van den Hurk, G. Lenderink, and A. P. Siebesma. *Technical Report 302: The KNMI regional atmospheric climate model RACMO version 2.1*. Royal Netherlands Meteorological Institute, De Bilt, 2008.

E. Van Meijgaard, L.H. van Ulft, G. Lenderink, S.R. de Roode, L. Wipfler, R. Boers, and R. M. A. Timmermans. Refinement and application of a regional atmospheric model for climate scenario calculations of Western Europe. *Climate Change Spatial Planning Publication*, KvR 054/12, 2012.

J. M. Van Wessem, C. H. Reijmer, J. T. M. Lenaerts, W. J. van de Berg, M. R. van den Broeke, and E. van Meijgaard. Updated cloud physics improve the modelled near-surface climate of Antarctica of a regional atmospheric climate model. *The Cryosphere*, 8:125 – 135, 2014. doi:10.5194/tc-8-125-2014.

P. W. White. Part IV : PHYSICAL PROCESSES (CY23R4). *Technical Report*, 2001.

B. Wouters, J. L. Bamber, M. R. van den Broeke, J. T. M. Lenaerts, and I. Sasgen. Limits in detecting acceleration of ice sheet mass loss due to climate variability. *Nature Geoscience*, 6:613 – 616, 2013. doi:10.1038/ngeo1874.

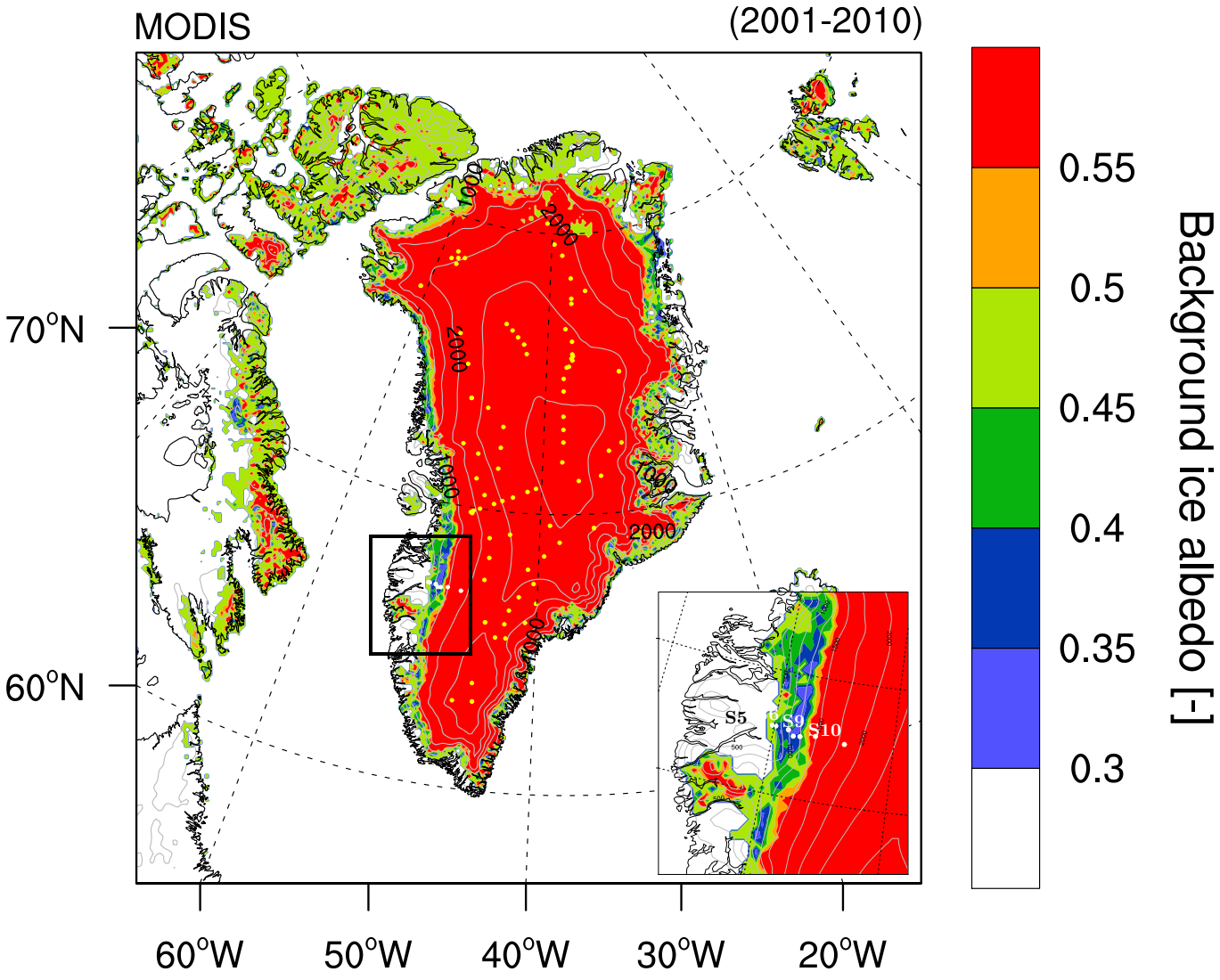

Fig. 1. MODIS background ice albedo prescribed in RACMO2.3. The RACMO2 integration domain is displayed as well as the location of the K-transect (white dots, see also inset) and accumulation zone sites (yellow dots).

AWS	S5	OBS.	RACMO2.1				RACMO2.3			
Variable	unit	mean	bias	σ_{bias}	RMSD	r^2	bias	σ_{bias}	RMSD	r^2
SW_d	W/m^2	108.7	16.3	18.7	24.8	0.98	26.2	20.8	33.4	0.99
SW_u	W/m^2	-69.8	-8.5	16.2	18.3	0.95	-15.4	18.4	24.0	0.93
LW_d	W/m^2	244.8	-17.2	8.6	19.2	0.97	-18.4	6.9	19.7	0.97
LW_u	W/m^2	-280.6	15.4	9.6	18.1	0.98	13.9	8.3	16.2	0.98
SHF	W/m^2	37.4	-11.8	19.7	23.0	0.21	-8.9	17.3	19.4	0.46
LHF	W/m^2	4.1	-2.6	5.3	5.9	0.60	-1.6	5.0	5.3	0.66
MELT	W/m^2	42.8	-7.8	17.7	19.4	0.96	-5.4	14.2	15.2	0.97
ALB	(-)	0.73	0.03	0.09	0.09	0.73	0.03	0.08	0.09	0.74
T_{2m}	°C	-6.0	-2.7	1.7	3.2	0.99	-2.3	1.1	2.6	0.99

Table 1. Modelled and observed annual mean SEB components and statistics of the differences (2004-2012) at station S5 (67°06' N, 50°05' W, 490 m a.s.l) in the ablation zone. Statistics include means of measurements collected at S5, model bias (RACMO2 - observations), standard deviation of the bias, Root Mean Square Difference (RMSD) of the bias as well as determination coefficient between RACMO2 and S5 observations. Fluxes are set positive for downward radiation.

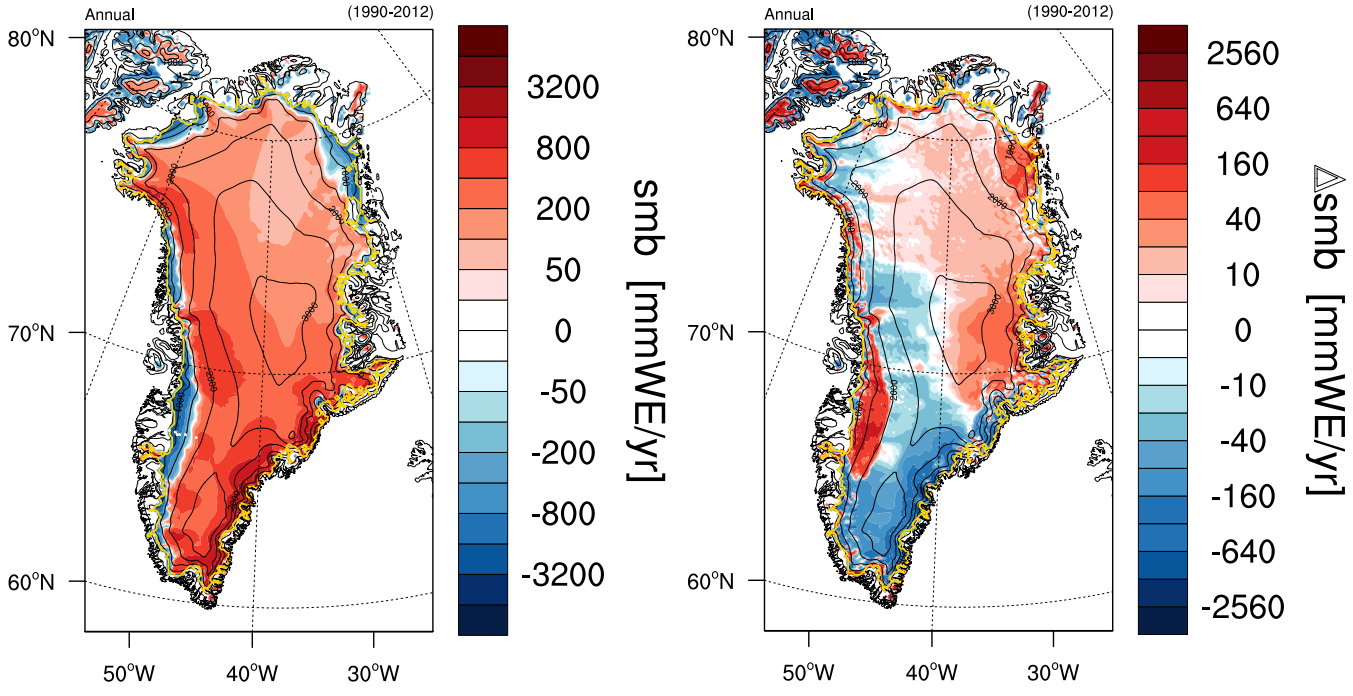

(a) RACMO2.3 (b) RACMO2.3 - RACMO2.1

Fig. 2. (a) Mean annual SMB (mmWE/yr) in RACMO2.3; (b) change in mean annual SMB (mmWE/yr) between RACMO2.3 and RACMO2.1 (1990-2012). The ice sheet margin is displayed in yellow.

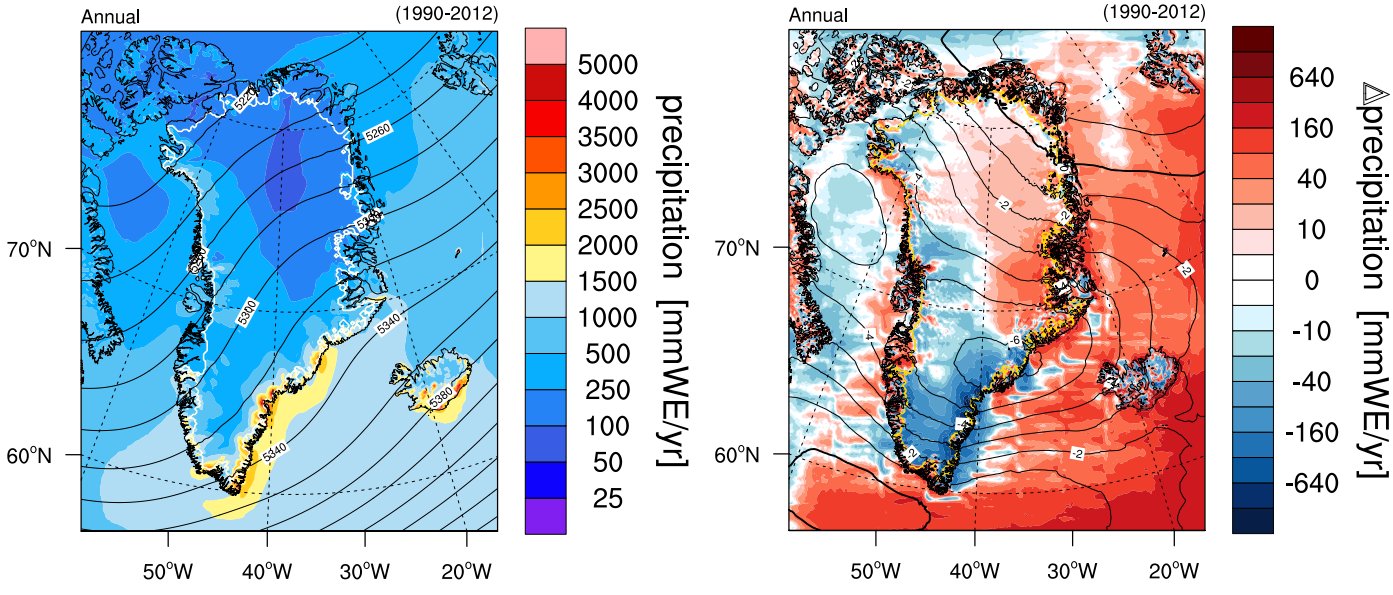

(a) RACMO2.3 (b) RACMO2.3 - RACMO2.1

Fig. 3. (a) Mean annual total (rain and snow) precipitation (mmWE/yr) and 500 hPa geopotential height (m) in RACMO2.3; (b) change in mean annual total precipitation (mmWE/yr) and 500 hPa geopotential height (m) between RACMO2.3 and RACMO2.1 (1990-2012).

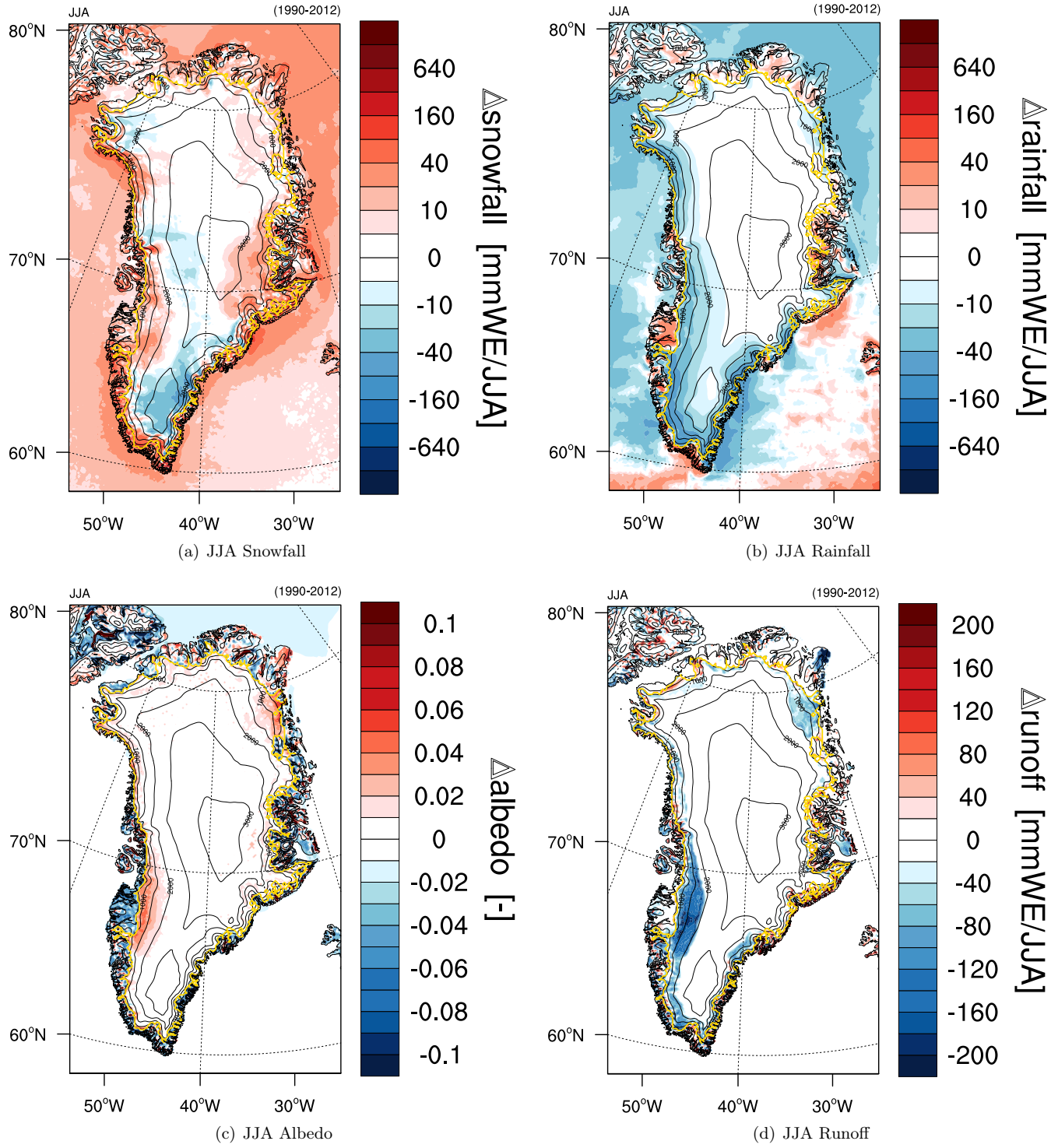

(a) JJA Snowfall (b) JJA Rainfall

(c) JJA Albedo (d) JJA Runoff

Fig. 4. Change in JJA mean (a) snowfall (mmWE/JJA), (b) rainfall (mmWE/JJA), (c) surface albedo and (d) runoff (mmWE/JJA) between RACMO2.3 and RACMO2.1 (1990-2012).

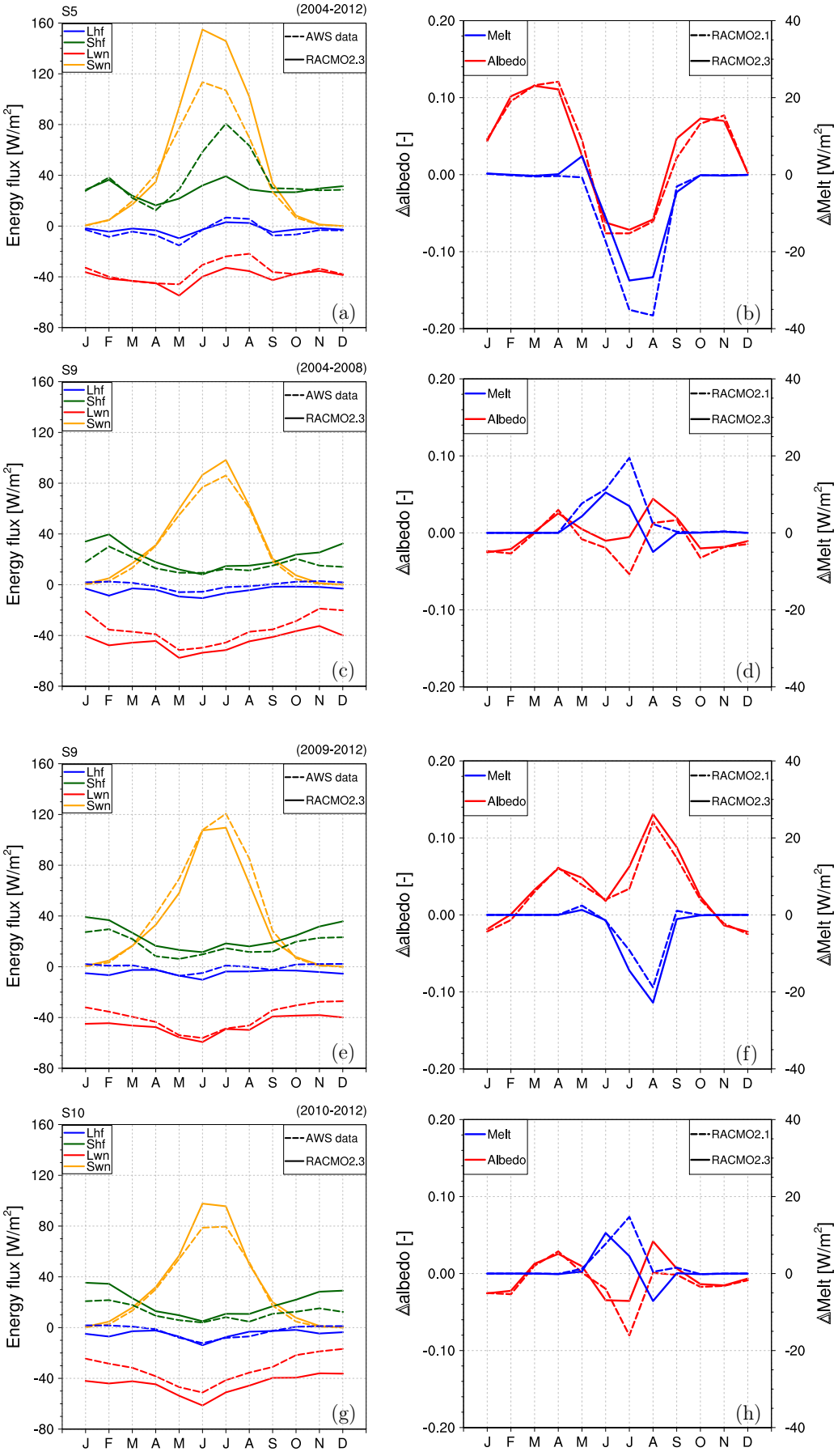

Fig. 5. Observed and modelled turbulent and net shortwave/longwave fluxes (W/m^2) at station (a) S5 for 2004-2012, (c) S9 for 2004-2008, (e) S9 for 2009-2012 and (g) S10 for 2010-2012; difference in modelled and observed surface albedo and surface melt energy (W/m^2) at stations (b) S5, (d) S9, (f) S9 and (h) S10 for the same periods.

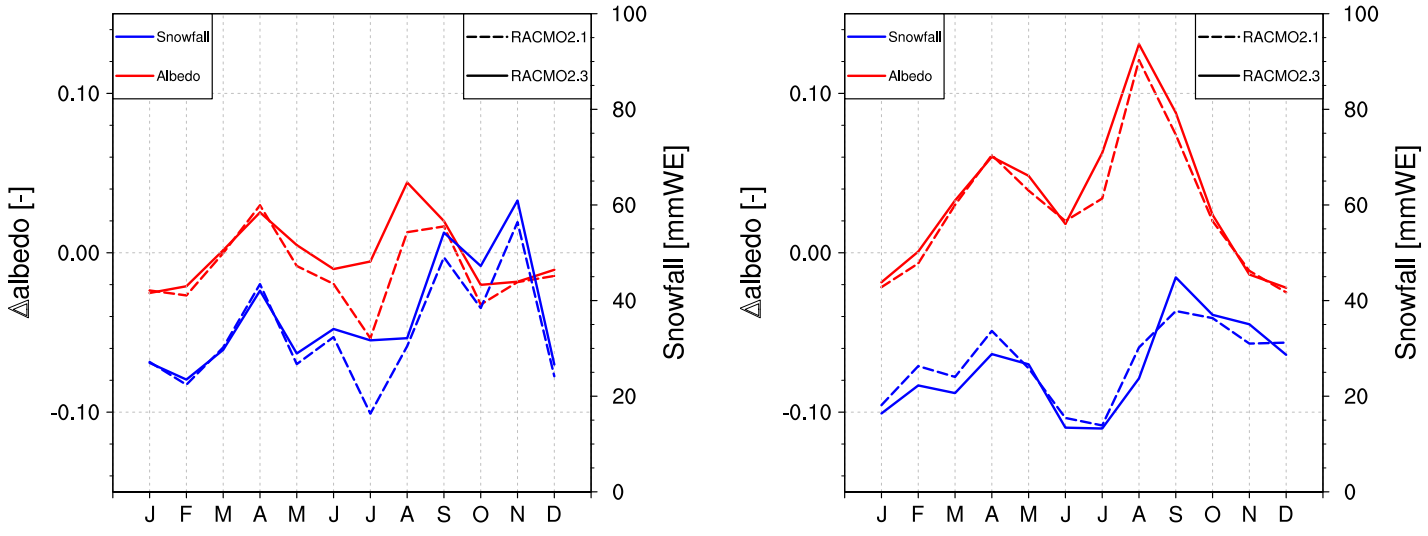

(a) S9 (2004-2008) (b) S9 (2009-2012)

Fig. 6. Differences in monthly mean surface albedo between models and S9 measurements, and monthly mean modelled snowfall for the periods (a) 2004-2008 and (b) 2009-2012.

AWS	S9	OBS.	RACMO2.1				RACMO2.3			
Variable	unit	mean	bias	σ_{bias}	RMSD	r^2	bias	σ_{bias}	RMSD	r^2
SW_d	W/m^2	139.8	-9.5	11.4	14.8	0.994	3.2	6.6	7.3	0.997
SW_u	W/m^2	-105.9	9.0	12.8	15.7	0.99	-3.3	9.1	9.7	0.99
LW_d	W/m^2	219.1	-9.1	12.4	15.4	0.92	-9.4	9.1	13.1	0.94
LW_u	W/m^2	-256.1	-0.2	4.5	4.5	0.99	1.1	3.9	4.1	0.99
SHF	W/m^2	16.5	9.8	7.5	12.4	0.61	6.6	5.8	8.8	0.69
LHF	W/m^2	0.3	4.3	3.1	5.3	0.34	4.4	3.4	5.6	0.28
MELT	W/m^2	12.6	1.0	9.2	9.2	0.86	-0.6	8.3	8.3	0.89
ALB	(-)	0.83	0.01	0.05	0.05	0.79	0.01	0.04	0.05	0.82
T_{2m}	°C	-13.0	0.6	0.9	1.1	0.99	0.1	0.7	0.7	0.99

Table 2. Same as Table 1 but for station S9 (67°03' N, 48°15' W, 1520 m a.s.l) close to the equilibrium line. SEB components include annual mean data for period 2004-2012.

AWS	S10	OBS.	RACMO2.1				RACMO2.3			
Variable	unit	mean	bias	σ_{bias}	RMSD	r^2	bias	σ_{bias}	RMSD	r^2
SW_d	W/m^2	141.5	-11.8	12.9	17.5	0.994	1.8	7.7	7.9	0.997
SW_u	W/m^2	-113.8	15.3	18.0	23.7	0.98	2.3	12.1	12.4	0.99
LW_d	W/m^2	220.4	-14.1	12.3	18.7	0.92	-14.1	8.9	16.7	0.93
LW_u	W/m^2	-252.5	0.6	5.2	5.2	0.98	1.6	4.2	4.5	0.99
SHF	W/m^2	11.9	11.6	7.7	13.9	0.64	7.9	5.7	9.8	0.74
LHF	W/m^2	2.7	1.5	3.8	4.1	0.41	2.5	4.0	4.7	0.39
MELT	W/m^2	8.9	2.1	5.9	6.2	0.94	0.7	4.3	4.3	0.94
ALB	(-)	0.86	-0.01	0.04	0.04	0.69	-0.001	0.04	0.04	0.71
T_{2m}	°C	-14.6	1.0	1.4	1.7	0.98	0.5	1.0	1.1	0.99

Table 3. Same as Table 1 but for station S10 (67°00' N, 47°01' W, 1850 m a.s.l) in the accumulation zone. SEB components include annual mean data for the period 2010-2012.

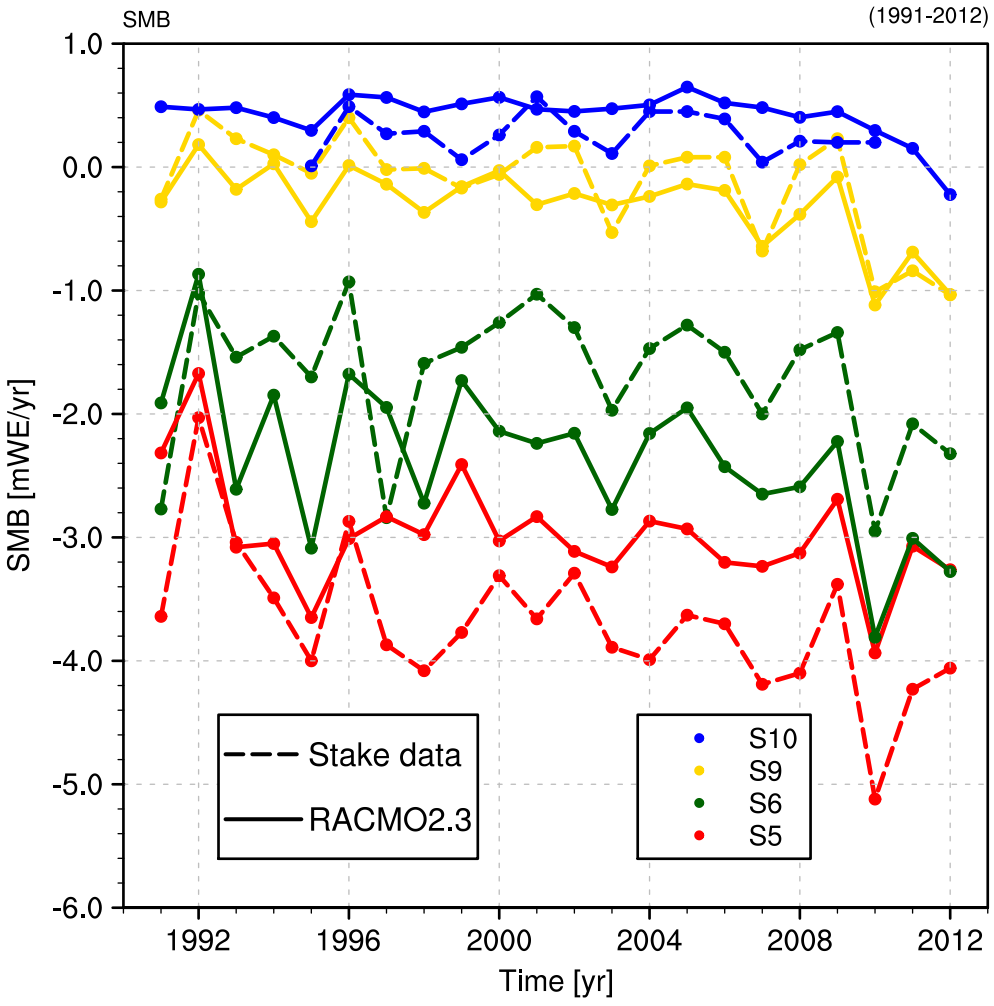

Fig. 7. Time series of observed (AWS) and modelled (RACMO2.3 and 2.1) annual mean SMB along the K-transect (mWE/yr) for the period 1991-2012.

Stakes	OBS.	RACMO2.1				RACMO2.3			
SMB	mean	bias	σ_{bias}	RMSD	r^2	bias	σ_{bias}	RMSD	r^2
S5	-3.7	1.0	0.5	1.1	0.36	0.7	0.4	0.8	0.49
SHR	-3.1	0.4	0.5	0.6	0.41	0.3	0.4	0.5	0.53
S6	-1.7	-0.8	0.6	1.0	0.25	-0.7	0.6	0.9	0.28
S7	-1.5	-0.7	0.4	0.9	0.59	-0.6	0.4	0.7	0.66
S8	-0.8	-0.7	0.4	0.8	0.55	-0.4	0.4	0.5	0.64
S9	-0.1	-0.4	0.2	0.5	0.73	-0.2	0.2	0.3	0.80
S10	0.3	-0.03	0.2	0.2	0.34	0.2	0.1	0.3	0.25

Table 4. Modelled and observed mean annual SMB (mWE/yr) and statistics of the differences at S5 (67°06' N, 50°05' W, 490 m a.s.l), SHR (67°06' N, 49°56' W, 710 m a.s.l), S6 (67°05' N, 49°24' W, 1010 m a.s.l), S7 (66°59' N, 49°09' W, 1110 m a.s.l), S8 (67°00' N, 48°53' W, 1260 m a.s.l) and S9 (67°03' N, 48°15' W, 1520 m a.s.l) over 1990-2012; S10 (67°00' N, 47°01' W, 1850 m a.s.l) covers the period 1994-2010.

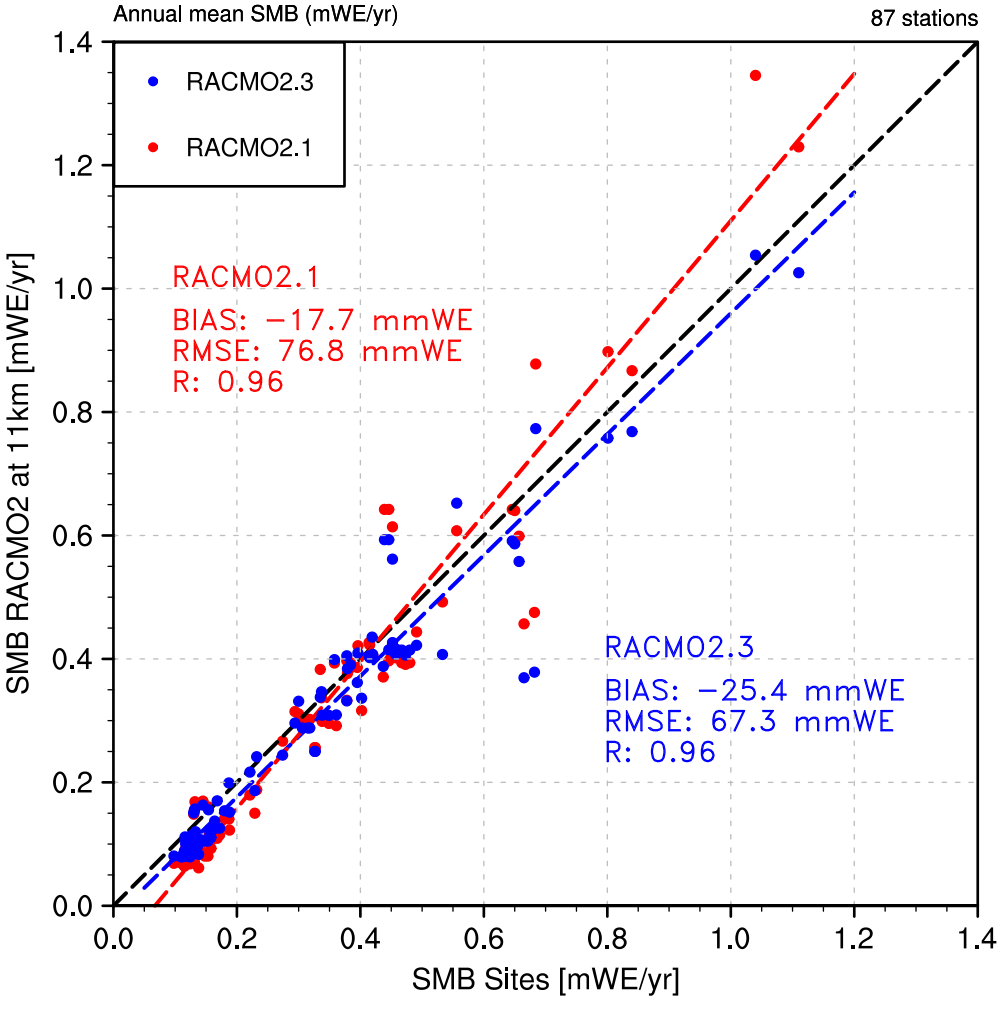

Fig. 8. Observed and simulated SMB (mWE/yr) across the accumulation zone of the GrIS averaged for the period 1979-2012. The regression lines are displayed as dashed lines for RACMO2.3 (blue) and 2.1 (red). For observation locations, see yellow dots in Fig. 1.

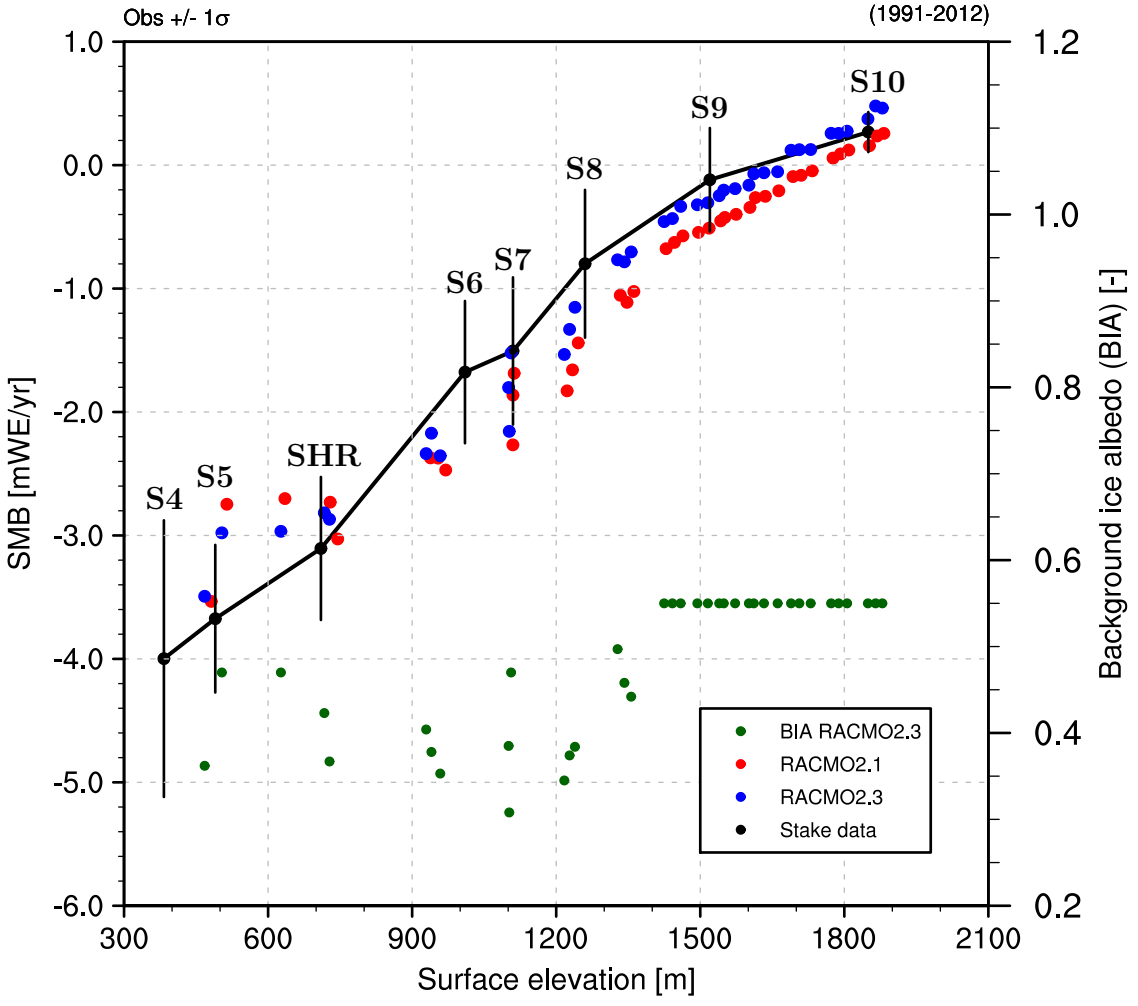

Fig. 9. Observed and simulated SMB (mWE/yr) along the K-transect in western Greenland ($\sim 67^{\circ}$N), averaged for the period 1991-2012. The observed SMB (black dots) at S4, S5, SHR, S6, S7, S8, S9 and S10 are based on annual stake measurements. S10 observations cover 1994-2010. The black bars represent the standard deviation ($\pm$ 1σ) around the 1991-2012 mean value. Modelled SMB at stake sites and intermediate locations are displayed for RACMO2.3 (blue dots) and RACMO2.1 (red dots). MODIS background ice albedo as prescribed in RACMO2.3, is depicted in green (axis on right).